Clustered Jamming in Aerial HetNets With Decoupled Access

MOHAMMAD ARIF[1], **SHURJEEL WYNE**[1], (Senior Member, IEEE),
KEIVAN NAVAIE[2], (Senior Member, IEEE),
MUHAMMAD SAJID HAROON[3], (Graduate Student Member, IEEE),
AND SADIA QURESHI[4]

[1]Department of Electrical and Computer Engineering, COMSATS University Islamabad (CUI), Islamabad 45550, Pakistan
[2]School of Computing and Communications, Lancaster University, Lancaster LA1 4WA, U.K.
[3]Telecommunications and Networking (TeleCoN) Research Laboratory, GIK Institute of Engineering Sciences and Technology, Topi 23640, Pakistan
[4]School of Data and Electrical Engineering, University of Technology Sydney, Sydney, NSW 2007, Australia

Corresponding author: Mohammad Arif (mohammadarif911@gmail.com)

ABSTRACT The tremendous increase in wireless connectivity demand will result in the degradation of the service quality and the scarcity of network capacity and coverage in the beyond 5th generation era. To ensure reliable connectivity and enhance the network's performance, the evolution of heterogeneous networks (HetNets) must incorporate aerial platforms in addition to traditional terrestrial base stations. The performance of Aerial-HetNets (A-HetNets) is largely dependent on the users' association. The conventional user-association scheme based on downlink received power provides sub-optimal performance for the edge users. For this reason, decoupled user-association along with the reverse frequency allocation (RFA) strategy has been employed in A-HetNets. The performance of A-HetNets is also affected if wide-band jammers (WBJs) are present in the vicinity and impose jamming interference. In this paper, a two-tier A-HetNet with RFA and decoupled access is analyzed in the presence of jamming interference. The obtained results show that for a signal-to-interference ratio threshold of -20 dBm, the percentage decrease in the coverage probability of the decoupled access due to WBJ activity is up to 7.4%, 13.5%, and 19.7%, for the average number of WBJs equal to 2, 4, and 6, respectively. The performance of the decoupled access in A-HetNets is further decreased by increasing the transmit power of the WBJs while it is increased by increasing the radius of the WBJ's cluster.

INDEX TERMS Downlink and uplink decoupling, heterogeneous networks, unmanned aerial vehicles, wide-band jammers.

I. INTRODUCTION

The evolution of 5th generation (5G) of wireless networks can increase the data demands, service types, and scale of wireless networks. It is estimated that the mobile-user and the machine-type subscribers would reach 17.1bn and 97bn, respectively, by the year 2030 [1]. Such massive increase will lead to the degradation in the quality of service (QoS) and scarcity of network capacity in the beyond 5G era [2]. Thus, to design networks in a cost-efficient manner, the evolution of base station (BS) coverage cells from macro- to femto- and pico-cells and from terrestrial-fixed to aerial-vehicular is

The associate editor coordinating the review of this manuscript and approving it for publication was Donatella Darsena.

indispensable. The aerial networks can use network resources more efficiently by creating favorable channel conditions or by extending the network's coverage for the target user equipment (UE) to meet the data demands for events, such as concerts, sports, disasters, and accidents.

A. MOTIVATION AND RELATED WORK

To maintain the QoS in ultra-high data demand environments, a promising solution is to deploy unmanned aerial vehicles (UAVs) [3]–[5]. The UAV-based BSs can provide the line-of-sight link to the target UE in aerial heterogeneous networks (A-HetNets). The appropriate deployment of UAVs encompasses numerous characterizations depending on their weight, trasnmit power, and size [6], [7]. The UAVs with the

functionalities such as low transmit power, less height, less endurance capability, and limited battery are usually considered as low-altitude platforms (LAPs). While, the UAVs with extended transmission power, higher altitude, and extensive endurance capability are considered as high-altitude platforms (HAPs).

The performance of HetNets is largely affected, if jammers are present in the vicinity and disrupt the legitimate transmission [8]–[10]. This performance is more vulnerable to jamming, if aerial BSs are present in the network. The target locations for jamming in A-HetNets are organizations, military-bases, air-ports, etc., where the jamming signal is typically introduced using wide-band jammer (WBJ). The main goal of the WBJs is to jam the legitimate uplink (UL) communication with unwanted energy (i.e., jamming interference) as effectively as possible. The transmission power of the WBJs is limited due to its wide-band nature, therefore, several WBJs (mostly present in clusters) are necessary to be located in the vicinity of the target [11].

The distribution of the WBJs in a cluster is considered more effective than the non-clustered distribution because it helps the jammers to obtain targets' network parameters such as frequency, location, and transmission power [11], [12]. Since the jammers are present in clusters, therefore, they can be modeled using a Matern cluster process (MCP). The authors in [13]–[16], modeled the A-HetNets using an MCP and showed that the design and performance gains of the network can be efficiently estimated by modeling the clustering process with an MCP.

Besides, the distribution of WBJs, user-association with the UAV also plays an important role in characterizing A-HetNets. Traditionally, the performance of A-HetNets is analyzed with the assumption that the target user is connected in downlink (DL) and UL with the same HAP by considering DL received power. However, this performance is sub-optimal for the edge users (e.g., users located at the boundary of a certain cell) which are associated to the HAP while, exhibiting a favorable channel condition to the LAP. Therefore, it is important to consider the user-association by exploiting the joint DL and UL access. To address this issue, *decoupled access* for A-HetNets is proposed, where the target UE is allowed to associate with the multiple UAVs based on joint DL and UL association [17]. In the decoupled accsss for A-HetNets, the target user connects to HAP in DL while to LAP in UL. Furthermore, in [18]–[20], the authors showed that in HetNets, the edge users can leverage better gains in terms of coverage probability, spectral- and energy-efficiency, if decoupled access is allowed. Nevertheless, in [20], the spectral efficiency performance for the traditional cellular networks under decoupled access in terms of Fox H-function is analyzed.[1] Therein, decoupled access for a multi-tier HetNet has shown improvement in performance gains over the the non-decoupled access.

---

[1] Fox H-function enables the analysis of the complex and infinite integrals. The Fox H-function is explained in terms of its implementation in [21].

An effective resource allocation strategy is reverse frequency allocation (RFA), whereby the HAP and LAP can use frequency resources in a reverse manner for DL and UL to attain better performance gains. The authors in [22], [23] showed that a multi-tier HetNet employing RFA strategy performs better than a multi-tier HetNet without RFA in terms of coverage. In this paper, we use RFA along with the decoupled access to improve networks' coverage performance by abating the inter-tier interference of multiple UAVs and the jamming interference of the WBJs.

Without decoupling, [24] analyzed a multi-tier A-HetNet which is similar to the traditional cellular HetNet. Therein, the HAPs and the LAPs are modeled using an independent and homogeneous Poisson point process (HPPP) and derived the analytical expression of the outage probability without considering RFA and decoupled access. Whereas, in [11], [25], the authors analyzed the coverage probability in conjunction with RFA, jammers, and decoupled access. This performance is limited due to the assumption that the same pathloss exponent is considered across all the tiers of a multi-tier cellular HetNet. Furthermore, the authors in [11] assumed that the jammers are always present in a single circular cluster around the target UE which is not a realistic approach as the jammers can be located in multiple-clusters and with different centers.

Our investigation is different from the recent works in the following.

- The authors in [24] present the analysis of a two-tier A-HetNet without considering the decoupled access. Further, their work lacks the analysis of RFA strategy in the presence of jammers.
- The authors in [17] investigate the performance of the decoupled access for a two-tier A-HetNet. However, their work lacks the joint analysis of RFA and jammers.
- The works in [11], [12], [25] analyzes HetNets by assuming the same pathloss exponents across the multiple tiers of a HetNet which is unrealistic and an oversimplified approach. In contrast, we employ a multi pathloss exponent model for multiple tiers of A-HetNets.
- The work in [25] investigates RFA, WBJs, and decoupled access for a conventional cellular HetNet. However, we employ RFA, WBJs and decoupled access for investigating a multi-tier A-HetNet.

B. MAIN CONTRIBUTIONS

In this paper, a multi-tier A-HetNet is analyzed by employing decoupled access in conjunction with RFA and WBJs. The WBJs are assumed to be present in multiple-clusters in the considered network and the decoupled access is employed by considering different pathloss exponents across a multi-tier A-HetNet. The summary of novel contributions is as follow:

- Investigating the UL coverage performance for the edge users in the presence of RFA and decoupled access.
- Mitigating the effect of WBJs and RFA on the performance of multi-tier A-HetNets with decoupled access.

- The analytical expression of the coverage probability in conjunction with RFA, WBJs, and decoupled access is derived for multi-tier A-HetNets.
- The performance of multi-tier A-HetNets is analyzed against network parameters, such as the transmit power of the LAP-associated UE, the transmit power of the WBJs, the radius of the WBJs cluster, and the transmit power of the LAPs.

The validity of the proposed analytical framework is established by conducting extensive simulations. The conducted analysis of the decoupled access with RFA stressed to WBJs in A-HetNets indicates a significant performance improvement when compared to the non-decoupled access in terms of coverage.

C. PAPER ORGANIZATION

The rest of this paper is organized in the following. Section II describes the system model for a two-tier A-HetNet in conjunction with RFA and WBJs, Section III describes the preliminaries related to target's association, target's distance distribution, and WBJ's interference, Section IV describes the coverage performance, Section V describes results and their discussion, and Section VI concludes this paper.

II. SYSTEM MODEL

In this paper, we enhance the system model adopted in our previous work in [17] by employing RFA in the presence of WBJs to investigate the performance of the decoupled A-HetNets in UL.

A. INFRASTRUCTURE DEPLOYMENT

Consider a two-tier A-HetNet, comprising of HAPs and LAPs as shown in Fig. 1. The HAPs and LAPs are distributed using an independent HPPP, i.e., Φ_H and Φ_L, with densities λ_H and λ_L, and heights h_H and h_L, respectively.

B. JAMMERS DEPLOYMENT

The transmit power of the WBJs is very low due to its wide-band nature. Since, in this paper, we focus on clustered jamming due to low transmit power levels, therefore, we assumed jamming due to WBJs. The WBJs are distributed using an MCP Φ_J with a density of λ_J. The MCP constits of parent and child nodes. The parent nodes are modeled using an independent HPPP with density λ_j. Whereas, the child nodes are independently and uniformly distributed in a cluster with radius r_j centered around each of the parent nodes. The parent nodes are excluded from the point process while the number of child nodes is a Poisson random variable. The probability density function (PDF) of the distance between the cluster center and the child node located at the location **a** within a cluster of radius r_j is given as [26]

$$f_m(\mathbf{a}) = \frac{1}{\pi r_j^2}, \quad \| \mathbf{a} \| \le r_j, \tag{1}$$

where $\| \mathbf{a} \|$ is the Euclidean distance between the cluster center and the child node. The child nodes are considered
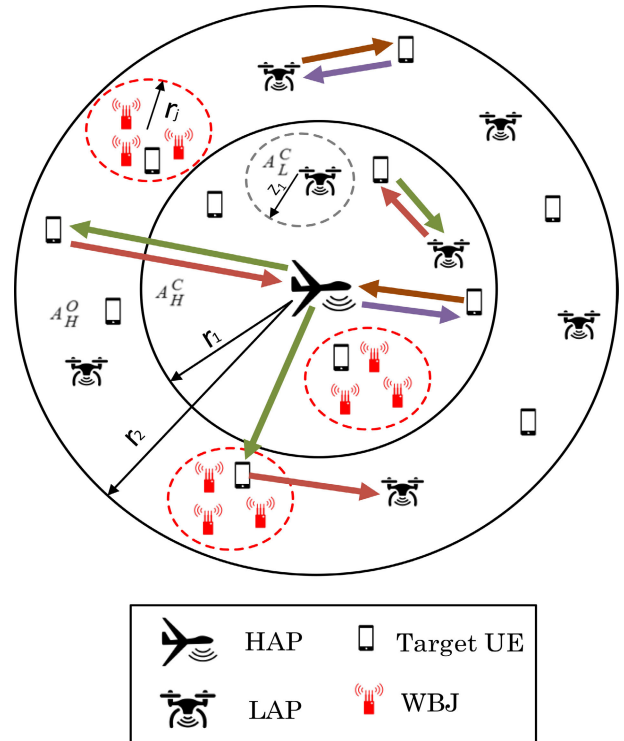
analogous to the WBJs and thus, can be distributed according to an MCP [13], [27]. Dissimilar to [11], where authors considered a worst case scenario in which WBJs are only present around the target UE; we model WBJs according to an MCP such that the WBJs are uniformly-distributed within a cluster. Furthermore, the density of WBJs in A-HetNets is given as $\lambda_J = \lambda_j \bar{c}$, where the average number of WBJs per cluster is $\bar{c}$.
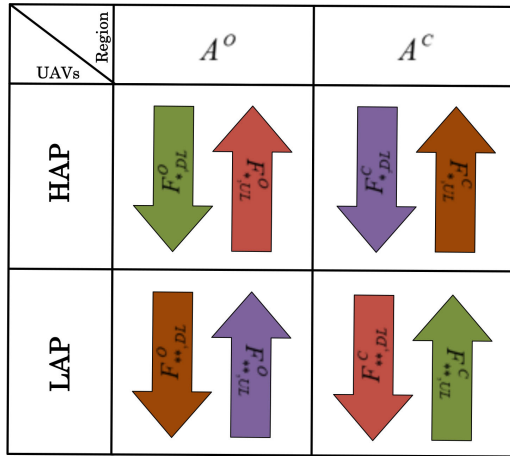
C. TARGET DEPLOYMENT

The users are distributed using an independent HPPP Φ_U with a density of λ_U. The UE whose UL legitimate communication is disrupted by the WBJs attacks is considered as a target UE. We deploy the target UE at the origin of the coordinate system. According to the Slivnyak's Theorem [28], placing a single point at the origin $x_o(0, 0, 0)$ of the coordinate system will not change the distribution of the point process.

D. BANDWIDTH ALLOCATION

We employ frequency reuse in a reverse manner for A-HetNets as shown in Fig. 2. Using RFA [22], [23], the whole range of frequencies in the DL of HAPs is made available in the UL of LAPs which helps to obtain a better coverage performance.

In RFA, we categorize frequencies associated to HAPs and LAPs as F_* and F_{**}, respectively. Each frequency describes two sub-bands based on their use-regions, i.e,. HAP- and LAP-enabled regions. For instance, the sub-bands

of HAP-enabled regions are F_*^C and F_*^O while the sub-bands of LAP-enabled regions are F_{**}^C and F_{**}^O. The HAP-enabled regions are those regions, where the target UE receives maximum transmit power from the HAP in the DL while in the UL, maximum transmit power is obtained by the same HAP from the target UE. Whereas, the LAP-enabled regions are those regions, where the target UE receives maximum transmit power from the LAP in the DL while in the UL, maximum transmit power is obtained by the same LAP from the target UE. The frequencies are further categorized based on their DL and UL access. For instance, $F_{*,DL}^C$, $F_{**,DL}^C$, $F_{*,DL}^O$, and $F_{**,DL}^O$ describe frequencies in the DL, while, $F_{*,UL}^C$, $F_{**,UL}^C$, $F_{*,UL}^O$, and $F_{**,UL}^O$ describe frequencies in the UL.

E. RECEIVED SIGNAL STRENGTH

The transmit power of the UAV and the UE associated with the tier, k is given as P_k and Q_k, respectively, where $k \in \{L, H\}$, while the power transmitted by the clustered jammers is given as P_j. The average transmit power obtained from the UAV connected to tier, k at the target UE is $\mathbb{E}\left\{ \mathsf{S}_k^{\mathrm{DL}} \right\} = P_k \parallel X_k \parallel^{-\alpha_k}$, where $\mathbb{E}\{.\}$ is the statistical expectation, $\alpha_k > 2$ is the pathloss exponent for the UAV associated to tier, k, and $\parallel X_k \parallel$ is the Euclidean distance between the origin and the UAV associated to tier, k. The power received from the target UE at the UAV connected to tier, k is given as $\mathbb{E}\left\{ \mathsf{S}_k^{\mathrm{UL}} \right\} = Q_k \parallel X_k \parallel^{-\alpha_k}$. We assume interference limited A-HetNets such that the interference power dominates the noise power.

We assume small scale Rayleigh fading gain between the k-th tier UAV and the UEs as $g_k \sim \exp(1)$. Furthermore, the channel is assumed to be static such that the UEs, UAVs, and WBJs are stationary for a particular environment. However, our model is valid for UAV-mobility transmissions. For detecting the transmitted signal successfully, τ is the signal-to-interference-ratio (SIR) threshold. Similar to [29], there is a single UE per UAV which acts as a dominant interferer in UL, such that the density of UEs is very high $\lambda_U \geq \lambda_H + \lambda_L$.

The UL SIR at the LAP by considering RFA in the presence of WBJs is expressed as

$$\mathrm{SINR}_L^{\mathrm{UL}} \triangleq \frac{Q_L g_L \parallel X_L \parallel^{-\alpha_L}}{\mathcal{I}_{\Phi_{L,A_H^O}}^{UL} + \mathcal{I}_{\Phi_{H,A_L^C}}^{DL} + \mathcal{I}_{\Phi_J}}, \quad (2)$$

where $\mathcal{I}_{\Phi_{L,A_H^O}}^{UL} = \sum_{i \epsilon \Phi_{I_{L,A_H^O}}} Q_L g_i \parallel X_i - X_L \parallel^{-\alpha_L}$ is the UL interference from the UEs located outside the HAP-enabled region A_H^O with the interference process Φ_{L,A_H^O}, $\mathcal{I}_{\Phi_{H,A_L^C}}^{DL} = \sum_{v \epsilon \Phi_{I_{H,A_L^C}}} P_H g_v \parallel X_v - X_H \parallel^{-\alpha_H}$ describes the DL interference of the HAPs from the LAP-enabled region A_L^C with interference process Φ_{H,A_L^C}, and $\mathcal{I}_{\Phi_J} = \sum_{l \epsilon \Phi_J} P_j g_l \parallel X_l - X_L \parallel^{-\alpha_L}$ describes the interference from the WBJs with interference process Φ_J.

Similarly, the UL SIR at the HAP by considering RFA in the presence of WBJs is expressed as

$$\mathrm{SINR}_H^{\mathrm{UL}} \triangleq \frac{Q_H g_H \parallel X_H \parallel^{-\alpha_H}}{\mathcal{I}_{\Phi_{H,A_H^O}}^{UL} + \mathcal{I}_{\Phi_{L,A_L^C}}^{DL} + \mathcal{I}_{\Phi_J}}, \quad (3)$$

where $\mathcal{I}_{\Phi_{H,A_L^O}}^{UL} = \sum_{i \epsilon \Phi_{I_{H,A_L^O}}} Q_H g_i \parallel X_i - X_H \parallel^{-\alpha_H}$ is the UL interference from the UEs located outside the HAP-enabled region A_H^O with the interference process Φ_{H,A_H^O}, $\mathcal{I}_{\Phi_{L,A_H^C}}^{DL} = \sum_{v \epsilon \Phi_{I_{L,A_H^C}}} P_L g_v \parallel X_v - X_L \parallel^{-\alpha_L}$ describes the DL interference of the LAPs from the LAP-enabled region A_L^C with interference process Φ_{L,A_L^C}, and $\mathcal{I}_{\Phi_J} = \sum_{l \epsilon \Phi_J} P_j g_l \parallel X_l - X_H \parallel^{-\alpha_H}$ describes the interference from the WBJs with interference process Φ_J.

III. PRELIMINARIES

Here, we present an overview for the UL and DL target's association criteria, the decoupled access, the distance distributions to the serving UAVs, and the interference at the serving UAV.

A. TARGET ASSOCIATION

In DL, the target UE is connected to the k-th tier UAV, T_k, based on maximum received signal strength in DL from that tier. Then, the location of location of the associated tier, T_k is given as [30]

$$T_k = arg \ \max_{k \epsilon (H,L)} P_k \parallel X_k \parallel^{-\alpha_k}.$$

While, in UL, the target UE is associated with the k-th tier UAV, T_k based on maximum received signal strength from that target UE at the k-th tier UAV. Then, the location of location of the associated tier, T_k is given as [30]

$$T_k = arg \ \max_{k \epsilon (H,L)} Q_k \parallel X_k \parallel^{-\alpha_k}.$$

The connection of the target UE with the UAV of tier, k defines that there isn't any other UAV located within a sphere of radius X_k, such that $\mathbb{P}\{X_k > x\} = e^{-\pi \lambda_k x^2}$ [28]. Further,
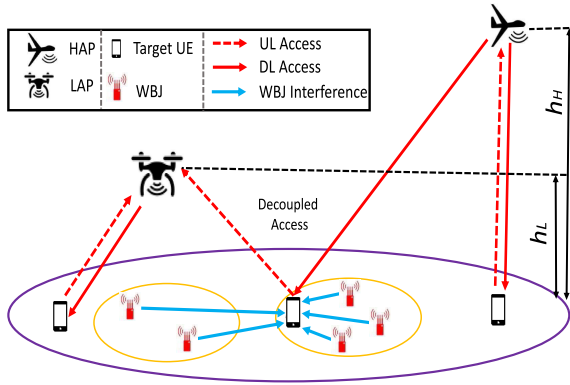
FIGURE 3. Decoupled access for the target user in A-HetNets [17].

the PDF distance between the target user and the serving UAV of tier, k is expressed as

$$f_{X_k}(x) = 2\pi\lambda_k x e^{-\pi\lambda_k x^2}, \quad x \geq 0. \tag{4}$$

B. DECOUPLED ACCESS

The connection of the target UE in DL with the HAP and in UL with the LAP will be considered as a decoupled access in the analysis to follow (see, Fig. 3). The UEs located in the regions that take part in the decoupled access are considered as "decoupled-enabled regions". In practical scenarios, the UEs located in the vicinity of cell-edge boundary facilitate decoupled access. Furthermore, the authors in [17], [20] showed that the decoupled access leverages better performance gains for the decoupled-enabled regions, therefore, we derive the association probability of the UEs located in the decoupled-enabled regions. The decoupled access for the decoupled-enabled regions is expressed as [17]

$$\mathcal{A}_D = \frac{\alpha_H}{2\alpha_L} \left(\mathcal{H}_{1,1}^{1,1} \left[\frac{\frac{\alpha_H}{\alpha_L}}{(\sqrt{\pi\lambda_H})} \left(\frac{Q_H}{Q_L}\right)^{\frac{1}{\alpha_L}} \middle| \begin{pmatrix} 0, \frac{1}{2} \end{pmatrix} \\ \sqrt{\pi\lambda_L} \right] - \mathcal{H}_{1,1}^{1,1} \left[\frac{(\sqrt{\pi\lambda_H})^{\alpha_H/\alpha_L} \left(\frac{P_H}{P_L}\right)^{1/\alpha_L}}{\sqrt{\pi\lambda_L}} \middle| \begin{pmatrix} 0, \frac{1}{2} \end{pmatrix} \\ \begin{pmatrix} 0, \frac{\alpha_H}{2\alpha_L} \end{pmatrix} \right] \right). \tag{5}$$

The proof of (5) is given in the Appendix (A).

C. DISTANCE DISTRIBUTION TO THE UAVs

Here, the distance distribution between the target UE and the serving UAV is derived. Since, the decoupled-enabled regions leverage better performance gains with the decoupled access, therefore, we focus to derive the distribution of the target UE located in the decoupled-enabled regions and the target user [20], [30]. For the target UE located in the decoupled-enabled

regions, its PDF distance to the serving LAP is expressed as [17]

$$f_{X_L}^{(D)}(x) = \left(\exp\left\{ -\pi\lambda_H \left(\frac{P_H}{P_L}\right)^{\frac{2}{\alpha_H}} x^{\frac{2\alpha_L}{\alpha_H}} \right\} \right.$$
$$\left. - \exp\left\{ -\pi\lambda_H \left(\frac{Q_H}{Q_L}\right)^{\frac{2}{\alpha_H}} x^{\frac{2\alpha_L}{\alpha_H}} \right\} \right) \frac{f_{X_L}(x)}{\mathcal{A}_D}. \tag{6}$$

Similarly, the PDF distance to the serving HAP is given as [17]

$$f_{X_H}^{(D)}(x) = \left(\exp\left\{ -\pi\lambda_L \left(\frac{P_L}{P_H}\right)^{\frac{2}{\alpha_L}} x^{\frac{2\alpha_H}{\alpha_L}} \right\} \right.$$
$$\left. - \exp\left\{ -\pi\lambda_L \left(\frac{Q_L}{Q_H}\right)^{\frac{2}{\alpha_L}} x^{\frac{2\alpha_H}{\alpha_L}} \right\} \right) \frac{f_{X_H}(x)}{\mathcal{A}_D}. \tag{7}$$

D. INTERFERENCE CHARACTERIZATION

Here, the interference at the serving UAV is analyzed and the Laplace transform of interference of LAPs, HAPs, UEs, and WBJs is derived.

1) RFA-BASED INTERFERENCE

Here, we derive the Laplace transform of the interference at the target UE based on the RFA scheme. In the decoupled access, the intended receiver in UL is the LAP while, in the non-decoupled access, the intended receiver is the HAP. Therefore, the Laplace transform of the interference for both the decoupled and the non-decoupled access under RFA is a unique expression and needs to be analyzed separately.

The Laplace transform of the interference for both the decoupled and the non-decoupled access can be sub-categorized into the Laplace transform of the UL and the Laplace transform of the DL interference. The Laplace transform of the UL interference for the decoupled access and by excluding the area of the HAP-enabled region is derived as

$$\mathcal{L}_{\mathcal{I}_{\Phi_{L,A_H^O}}^{UL}}(s)$$
$$\overset{a}{=} \mathbb{E}_{\mathcal{I}_{\Phi_{L,A_H^O}}^{UL}}\left\{\exp(-\mathcal{I}_{\Phi_{L,A_H^O}}^{UL} s)\right\}$$
$$\overset{b}{=} \mathbb{E}_{\mathcal{I}_{\Phi_{L,A_H^O}}^{UL},g_i}\left\{\exp(-\frac{\tau x^{\alpha_L}}{Q_L} \sum_{i\in\Phi_{I_{L,A_H^O}}} Q_L g_i r_i^{-\alpha_L})\right\}$$
$$\overset{c}{=} \mathbb{E}_{\mathcal{I}_{\Phi_{L,A_H^O}}^{UL}}\left\{ \prod_{i\in\Phi_{I_{L,A_H^O}}} \mathbb{E}_{g_i}\left\{\exp(-x^{\alpha_L} g_i r_i^{-\alpha_L})\right\} \right\}$$

$$\stackrel{d}{=} \mathbb{E}_{\mathcal{I}^{UL}_{\Phi_{L,A^O_H}}} \left\{ \prod_{i \epsilon \Phi_{L,A^O_H}} \frac{1}{1 + \tau \left(\frac{r_i}{x} \right)^{-\alpha_L}} \right\}$$

$$\stackrel{e}{=} \exp \left\{ -2\pi \lambda_L \int_{r_1}^{r_2} \frac{r_i dr_i}{1 + \left(\frac{r_i}{\tau^{1/\alpha_L} x} \right)^{\alpha_L}} \right\}$$

$$\stackrel{f}{=} \exp \left\{ -\pi \lambda_L \tau^{2/\alpha_L} x^2 \int_{\left(\frac{r_1}{\tau^{1/\alpha_L} x} \right)^2}^{\left(\frac{r_2}{\tau^{1/\alpha_L} x} \right)^2} \frac{dw}{1 + w^{\alpha_L/2}} \right\}$$

$$\stackrel{g}{=} \exp \left\{ \frac{2\pi \lambda_L \tau r_2^{2-\alpha_L}}{x^{-\alpha_L}(\alpha_L - 2)} {}_2F_1 \left(1, 1 - \frac{2}{\alpha_L}; 2 - \frac{2}{\alpha_L}; -\tau \left(\frac{x}{r_2} \right)^{\alpha_L} \right) \right.$$
$$\left. - \frac{2\pi \lambda_L \tau r_1^{2-\alpha_L}}{x^{-\alpha_L}(\alpha_L - 2)} {}_2F_1 \left(1, 1 - \frac{2}{\alpha_L}; 2 - \frac{2}{\alpha_L}; -\tau \left(\frac{x}{r_1} \right)^{\alpha_L} \right) \right\}. \quad (8)$$

Here, $\stackrel{a}{=}$ is obtained using the Laplace transform definition, where $s = \frac{\tau x^{\alpha_L}}{Q_L}$, $\stackrel{b}{=}$ is obtained by substituting s and $\mathcal{I}^{UL}_{\Phi_{L,A^O_H}}$, $\stackrel{c}{=}$ follows by simple mathematical manipulations, $\stackrel{d}{=}$ follows by employing the Laplace transform of the interference w.r.t. g_i, $\stackrel{e}{=}$ follows by the probability generation functional (PGFL) of HPPP [31], where r_1 and r_2 is the radius of $\mathcal{A}^C_H$ and $\mathcal{A}^O_H$, respectively, $\stackrel{f}{=}$ follows by substituting $w = \left(\frac{r_i}{\tau^{1/\alpha_L} x} \right)^2$ in $\stackrel{e}{=}$, $\stackrel{g}{=}$ follows by solving the integration, where ${}_2F_1(-, -; -; -)$ is a Hypergeometric function [32].

Similarly, following the same steps, the Laplace transform of the interference in UL from outside the HAP-enabled region and with the non-decoupled access can be derived as

$$\mathcal{L}_{\mathcal{I}^{UL}_{\Phi_{H,A^O_H}}}(s)$$
$$= \exp \left\{ \frac{2\pi \lambda_H \tau r_2^{2-\alpha_H}}{x^{-\alpha_H}(\alpha_H - 2)} {}_2F_1 \left(1, 1 - \frac{2}{\alpha_H}; 2 - \frac{2}{\alpha_H}; -\tau \left(\frac{x}{r_2} \right)^{\alpha_H} \right) \right.$$
$$\left. - \frac{2\pi \lambda_H \tau r_1^{2-\alpha_H}}{x^{-\alpha_H}(\alpha_H - 2)} {}_2F_1 \left(1, 1 - \frac{2}{\alpha_H}; 2 - \frac{2}{\alpha_H}; -\tau \left(\frac{x}{r_1} \right)^{\alpha_H} \right) \right\}. \quad (9)$$

Furthermore, the DL interference in terms of the Laplace transform of the interference for the LAP-enabled region and with the decoupled access can be derived as

$$\mathcal{L}_{\mathcal{I}^{DL}_{\Phi_{H,A^C_L}}}(s)$$
$$= \exp \left\{ \frac{2\pi \zeta_L^H \lambda_H \tau z_1^{2-\alpha_H}}{x^{-\alpha_H}(\alpha_H - 2)} {}_2F_1 \left(1, 1 - \frac{2}{\alpha_H}; 2 - \frac{2}{\alpha_H}; \right. \right.$$
$$\left. -\zeta_L^H \tau \left(\frac{x}{z_1} \right)^{\alpha_H} \right) - \frac{2\pi \zeta_L^H \lambda_H \tau z_0^{2-\alpha_H}}{x^{-\alpha_H}(\alpha_H - 2)} {}_2F_1 \left(1, 1 - \frac{2}{\alpha_H}; 2 \right.$$
$$\left. \left. - \frac{2}{\alpha_H}; -\zeta_L^H \tau \left(\frac{x}{z_0} \right)^{\alpha_H} \right) \right\}. \quad (10)$$

Here, z_0 and z_1 are the lower and the upper limits for the LAP-enabled region. $\zeta_L^H = \frac{P_H}{Q_L}$ corresponds to the ratio of the transmit power of the HAP to the transmit power of the UE associated with the LAP, where the subscript in ζ_L^H represents the DL power of the UAV and the subscript in ζ_L^H represents the UL transmit power of the UE connected to the serving UAV.

Similarly, following the same procedure, the DL interference in terms of the Laplace transform of the interference for the LAP-enabled region and with the non-decoupled access can be derived as

$$\mathcal{L}_{\mathcal{I}^{DL}_{\Phi_{L,A^C_L}}}(s)$$
$$= \exp \left\{ \frac{2\pi \zeta_H^L \lambda_L \tau z_1^{2-\alpha_L}}{x^{-\alpha_L}(\alpha_L - 2)} {}_2F_1 \left(1, 1 - \frac{2}{\alpha_L}; 2 - \frac{2}{\alpha_L}; -\zeta_H^L \tau \left(\frac{x}{z_1} \right)^{\alpha_L} \right) \right.$$
$$\left. - \frac{2\pi \zeta_H^L \lambda_L \tau z_0^{2-\alpha_L}}{x^{-\alpha_L}(\alpha_L - 2)} {}_2F_1 \left(1, 1 - \frac{2}{\alpha_L}; 2 - \frac{2}{\alpha_L}; -\zeta_H^L \tau \left(\frac{x}{z_0} \right)^{\alpha_L} \right) \right\}. \quad (11)$$

2) CLUSTER-BASED INTERFERENCE

Here, the interference from the WBJs is characterized for the k-th tier UAV in terms of the Laplace transform of the interference. Consider $\upsilon(x) = \mathcal{L}_{\mathcal{I}_{\Phi_j}}(s)$, where $s = \frac{x_k^\alpha \tau}{Q_k}$, then using [26], [33], the interference of the k-th tier UAV in UL is expressed by the PGFL, $G(\upsilon)$ and the conditional PGFL, $\wp(\upsilon)$ and is expressed as

$$\wp(\upsilon) = \mathbb{E} \{ \Pi_{x \epsilon \Phi} \upsilon(x) \}$$
$$= G(\upsilon) \times \mho, \quad (12)$$

where

$$\mho \triangleq \exp \left\{ -\frac{P_j x^2 \tau^{2/\alpha_k} 2\pi \bar{c}}{Q_k \alpha_k r_j^2} \csc \left(\frac{2\pi}{\alpha_k} \right) \right\}. \quad (13)$$

The PGFL is solved for the pathloss exponent $\alpha_k > 2$. Thus, for the MCP distributed jammers, $G(\upsilon)$ is given as

$$G(\upsilon)$$
$$= \exp \left\{ -\lambda_j \pi \frac{P_j \tau^{2/\alpha_k} x^2}{Q_k} \int_0^\infty \left(1 - \exp \left\{ \frac{-\bar{c}}{1 + t^{\alpha_k/2}} \right\} \right) dt \right\}. \quad (14)$$

Then, substituting (13) and (14) in (12) and assuming $\Delta_k = \frac{P_j}{Q_k}$, the interference of the WBJs is obtained as the following.

$$\mathcal{L}_{\mathcal{I}_{\Phi_j}}(s)$$
$$= \exp \left\{ -\frac{2\pi \bar{c} \Delta_k x^2 \tau^{2/\alpha_k}}{\alpha_k r_j^2} \csc \left(\frac{2\pi}{\alpha_k} \right) \right.$$
$$\left. -\lambda_j \pi \Delta_k \tau^{2/\alpha_k} x^2 \int_0^\infty \left(1 - \exp \left\{ \frac{-\bar{c}}{1 + t^{\alpha_k/2}} \right\} \right) dt \right\}. \quad (15)$$

IV. COVERAGE PROBABILITY ANALYSIS

The probability that the serving UAV in the presence of WBJs receives an SIR larger than the SIR threshold is considered as coverage probability in UL. The coverage probability in UL for the UAV associated to tier, k is given as

$$C \triangleq \mathbb{E}_{X_k} \left\{ \mathbb{P}\{\text{SIR}_{X_k}^{\text{UL}} > \tau\} \right\}. \tag{16}$$

The coverage probability of the decoupled access in UL is the probability that the LAP in the presence of WBJs receives an SIR larger than the SIR threshold. In conjunction with the RFA, WBJs, and decoupled access, the coverage probability in UL is derived as [11], [23]

$$
\begin{aligned}
C^{\mathcal{D}} &\triangleq \int_{r_1}^{r_2} \mathbb{P}\{\text{SIR}_{X_L}^{\text{UL}} > \tau\} f_{X_L}^{(D)}(x) dx \\
&\overset{a}{=} \int_{r_1}^{r_2} \mathbb{P}\left\{ \frac{Q_L g_L \parallel X_L \parallel^{-\alpha_L}}{\mathcal{I}_{\Phi_{L,A_H^O}}^{\text{UL}} + \mathcal{I}_{\Phi_{H,A_L^C}}^{\text{DL}} + \mathcal{I}_{\Phi_J}} > \tau \right\} f_{X_L}^{(D)}(x) dx \\
&\overset{b}{=} \int_{r_1}^{r_2} \mathbb{E}\left\{ g_L > \frac{\tau x^{\alpha_L}}{Q_L} \left(\mathcal{I}_{\Phi_{L,A_H^O}}^{\text{UL}} + \mathcal{I}_{\Phi_{H,A_L^C}}^{\text{DL}} + \mathcal{I}_{\Phi_J} \right) \right\} \\
&\qquad \times \quad f_{X_L}^{(D)}(x) dx \\
&\overset{c}{=} \int_{r_1}^{r_2} \mathbb{E}\left\{ \exp\left(-s\mathcal{I}_{\Phi_{L,A_H^O}}^{\text{UL}} \right) \right\} \mathbb{E}\left\{ \exp\left(-s\mathcal{I}_{\Phi_{H,A_L^C}}^{\text{DL}} \right) \right\} \\
&\qquad \times \mathbb{E}\left\{ \exp\left(-s\mathcal{I}_{\Phi_J} \right) \right\} f_{X_L}^{(D)}(x) dx \\
&\overset{d}{=} \int_{r_1}^{r_2} \mathcal{L}_{\mathcal{I}_{\Phi_{L,A_H^O}}^{\text{UL}}}(s) \mathcal{L}_{\mathcal{I}_{\Phi_{H,A_L^C}}^{\text{DL}}}(s) \mathcal{L}_{\mathcal{I}_{\Phi_j}}(s) f_{X_L}^{(D)}(x) dx, \quad (17)
\end{aligned}
$$

where $\overset{a}{=}$ follows by substituting (2), $\overset{b}{=}$ follows by simple mathematical manipulations, $\overset{c}{=}$ follows by substituting $s = \dfrac{\tau x^{\alpha_L}}{Q_L}$ and exploiting the exponentially distributed gains due to Rayleigh fading, and $\overset{d}{=}$ follows by the definition of Laplace transform of interference. Finally, the UL coverage probability of the target UE with RFA, WBJs, and decoupled access

is obtained by substituting (8), (10), (15), and (6) in (17) and is expressed in (20), as shown at the bottom of the page.

The probability that the HAP in the presence of WBJs receives an SIR larger than the SIR threshold is considered as the non-decoupled UL coverage probability. In conjunction with RFA, WBJs, and non-decoupled access, the UL coverage probability is derived as

$$C^{\mathcal{ND}} \triangleq \mathbb{E}_{X_H} \left\{ \mathbb{P}\{\text{SIR}_{X_H}^{\text{UL}} > \tau\} \right\}. \tag{18}$$

Similar to (17), the UL coverage probability with RFA and WBJs for the non-decoupled access can be expressed as

$$C^{\mathcal{ND}} = \int_{r_1}^{r_2} \mathcal{L}_{\mathcal{I}_{\Phi_{H,A_H^O}}^{\text{UL}}}(s) \mathcal{L}_{\mathcal{I}_{\Phi_{L,A_L^C}}^{\text{DL}}}(s) \mathcal{L}_{\mathcal{I}_{\Phi_j}}(s) f_{X_L}^{(D)}(x) dx, \tag{19}$$

The final expression of the UL coverage probability in conjunction with RFA, WBJs, and non-decoupled access can be obtained by substituting the values of (9), (11), (15), and (7) in (19) and is expressed in (21), as shown at the bottom of the page.

V. RESULTS AND DISCUSSION

Here, a two-tier A-HetNet is analyzed by employing RFA in the presence of WBJs. The results are obtained by 100, 000 independent Monte-Carlo trials using the simulation parameters listed in Table 1.

The coverage probability of the decoupled access (DUDe-labeled curve) is better than the non-decoupled access (labeled as Non-DUDe) as shown in Fig. 4. This is due to the fact that the distance-dependent pathloss between the LAP and the target user is smaller than the distance-dependent pathloss between the HAP and the target user which results in higher UL SIR and the coverage probability. It is observed that the coverage probability decreases with the increase in the number of WBJs because each WBJ introduces jamming interference which compromises legitimate UL communication. The approximate percentage decrease in the coverage

$$
\begin{aligned}
C^{\mathcal{D}} &= \int_{r_1}^{r_2} \exp\left(\pi \tau x^{\alpha_L} \left[\frac{\lambda_L}{\alpha_L/2-1} r_2^{2-\alpha_L} {}_2F_1(1, 1-\frac{2}{\alpha_L}; 2-\frac{2}{\alpha_L}; -\tau \left(\frac{x}{r_2}\right)^{\alpha_L}) - \frac{\lambda_L}{\alpha_L/2-1} r_1^{2-\alpha_L} {}_2F_1(1, 1-\frac{2}{\alpha_L}; 2-\frac{2}{\alpha_L}; -\tau \left(\frac{x}{r_1}\right)^{\alpha_L}) \right. \right. \\
&\left. + \frac{\lambda_H}{\alpha_H/2-1} \zeta_L^H z_1^{2-\alpha_H} {}_2F_1(1, 1-\frac{2}{\alpha_H}; 2-\frac{2}{\alpha_H}; -\zeta_L^H \tau \left(\frac{x}{z_1}\right)^{\alpha_H}) - \frac{\lambda_H}{\alpha_H/2-1} \zeta_L^H z_0^{2-\alpha_H} {}_2F_1(1, 1-\frac{2}{\alpha_H}; 2-\frac{2}{\alpha_H}; -\zeta_L^H \tau \left(\frac{x}{z_0}\right)^{\alpha_H}) \right] \\
&\left. - x^2 \Delta_L \tau^{2/\alpha_L} \frac{2\pi\bar{c}}{\alpha_L r_j^2} \csc\left(\frac{2\pi}{\alpha_L}\right) - \lambda_j \pi \tau^{2/\alpha_L} \Delta_L x^2 \int_0^\infty \left(1 - \exp\left\{ \frac{-\bar{c}}{1+t^{\alpha_L/2}} \right\}\right) dt \right) f_{X_L}^{(D)}(x) x dx. \tag{20}
\end{aligned}
$$

$$
\begin{aligned}
C^{\mathcal{ND}} &= \int_{r_1}^{r_2} \exp\left(\pi \tau x^{\alpha_H} \left[\frac{2\lambda_H}{\alpha_H-2} r_2^{2-\alpha_H} {}_2F_1(1, 1-\frac{2}{\alpha_H}; 2-\frac{2}{\alpha_H}; -\tau \left(\frac{x}{r_2}\right)^{\alpha_H}) - \frac{2\lambda_H}{\alpha_H-2} r_1^{2-\alpha_H} {}_2F_1(1, 1-\frac{2}{\alpha_H}; 2-\frac{2}{\alpha_H}; -\tau \left(\frac{x}{r_1}\right)^{\alpha_H}) \right. \right. \\
&\left. + \frac{2\lambda_L}{\alpha_L-12} \zeta_H^L z_1^{2-\alpha_L} {}_2F_1(1, 1-\frac{2}{\alpha_L}; 2-\frac{2}{\alpha_L}; -\zeta_H^L \tau \left(\frac{x}{z_1}\right)^{\alpha_L}) - \frac{2\lambda_L}{\alpha_L-2} \zeta_H^L z_0^{2-\alpha_L} {}_2F_1(1, 1-\frac{2}{\alpha_L}; 2-\frac{2}{\alpha_L}; -\zeta_H^L \tau \left(\frac{x}{z_0}\right)^{\alpha_L}) \right] \\
&\left. - x^2 \Delta_H \tau^{2/\alpha_H} \frac{2\pi\bar{c}}{\alpha_H r_j^2} \csc\left(\frac{2\pi}{\alpha_H}\right) - \lambda_j \pi \tau^{2/\alpha_H} \Delta_H x^2 \int_0^\infty \left(1 - \exp\left\{ \frac{-\bar{c}}{1+t^{\alpha_H/2}} \right\}\right) dt \right) f_{X_H}^{(D)}(x) x dx. \tag{21}
\end{aligned}
$$

TABLE 1. Simulation parameters for the considered A-HetNets.

Notation	Description	Value
λ_H	HAP density	$1/\pi 1000^2$ m^{-2}
λ_L	LAP density	$2\lambda_H$
α_H	HAP pathloss exponent	2.75
α_L	LAP pathloss exponent	3
P_H	HAP transmit power	46 dBm
P_L	LAP transmit power	30 dBm
P_j	WBJ transmit power	10 dBm
Q_H	Transmit power of the HAP-associated UE	30 dBm
Q_L	Transmit power of the LAP-associated UE	30 dBm
h_H	HAP height	300 m
h_L	LAP height	100 m
$\bar{c}$	Average WBJs per cluster	4
λ_j	Parent clusters of WBJ	$1/\pi 1000^2$ m^{-2}
r_j	Cluster radius	100 m
τ	SIR threshold	-20 dB
B	System bandwidth	20 MHz

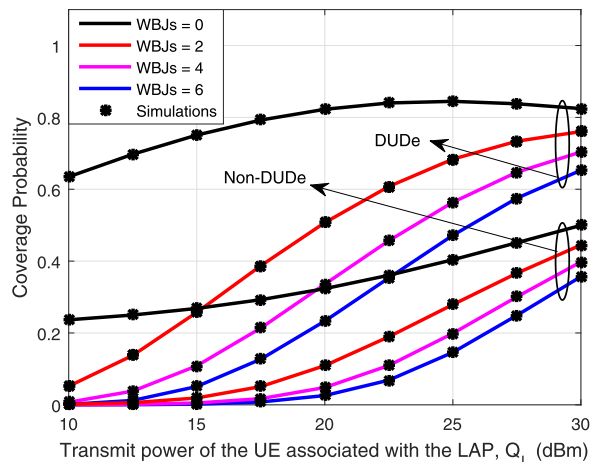**FIGURE 4.** UL coverage probability against τ, for different number of WBJs.

FIGURE 5. UL coverage probability against Q_L, for different number of WBJs.

decoupled access increases up to 0.75, 0.7, and 0.65, for the average number of WBJs equal to 2, 4, and 6, respectively. For the increase in the transmit power of UE associated with the LAP from 20 dBm to 30 dBm and for the average number of WBJs equal to 2, 4, and 6, the percentage increase in the coverage probability of the decoupled access is equal to 33.3%, 53.5%, and 65.3%, respectively.
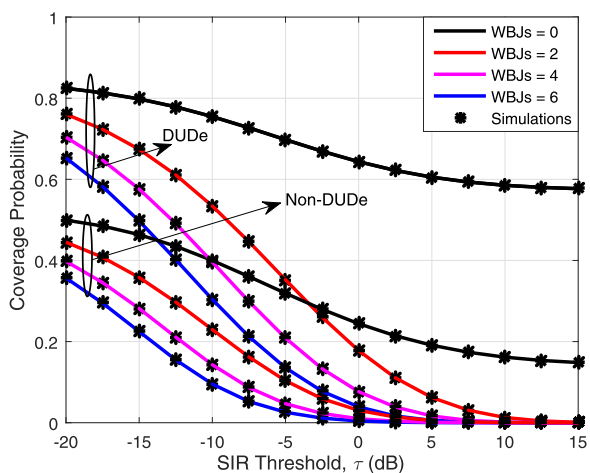

FIGURE 6. UL coverage probability against P_j, for different number of WBJs.

The coverage probability decreases by increasing the transmit power of the WBJs as shown in Fig. 6. This is because of the fact that each WBJ increases its transmit power to increase the jamming interference in the network. This results in the overall reduction of the UL SIR and the UL coverage probability. For instance, the coverage probability of the decoupled access by considering the transmit power of the WBJs equal to 5 dBm and with the average number of WBJs equal to 2, 4, and 6 is equal to 0.8, 0.79, and 0.78, respectively, while, by considering the transmit power of the WBJs equal to 10 dBm, the coverage probability of the decoupled access decreases up to 0.75, 0.7, and 0.65, for the average number of

probability of the decoupled access due to WBJ activity for the SIR threshold of -20 dBm is equal to 7.4%, 13.5%, and 19.7%, for the average number of WBJs equal to 2, 4, and 6, respectively.

The coverage probability increases by increasing the transmit power of the UE associated with the LAP as shown in Fig. 5. This may be due to the fact that more users are added in the decoupled-enabled regions. Furthermore, a significant increase in the coverage probability of the decoupled access is observed for the WBJs activity. For instance, by considering the transmit power of the user associated with the LAP equal to 20 dBm and with the average number of WBJs of 2, 4, and 6, the coverage probability of the decoupled access in UL is equal to 0.5, 0.325, and 0.225, respectively, while, by considering the transmit power of the user associated with the LAP equal to 30 dBm, the coverage probability of the
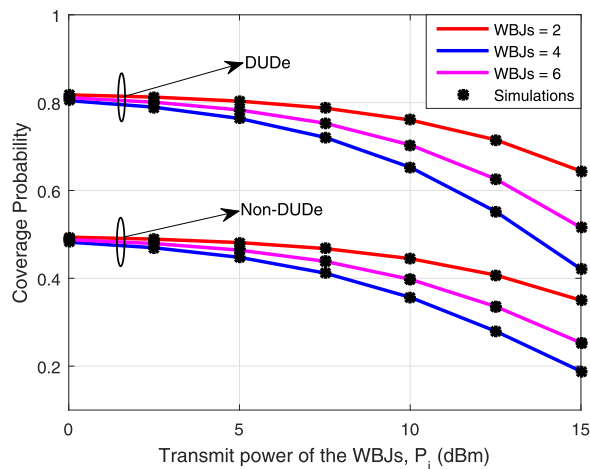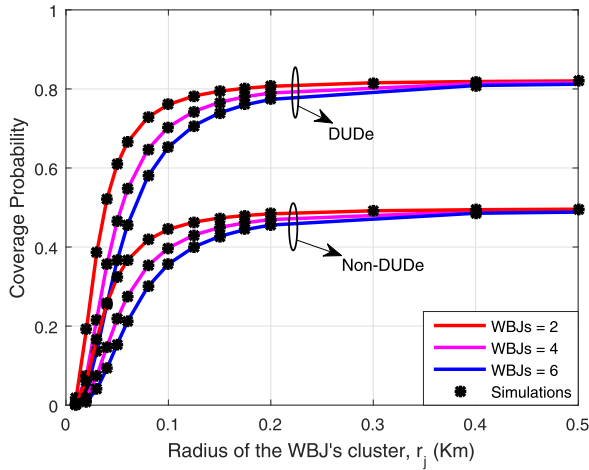
FIGURE 7. UL coverage probability against r_j, for different number of WBJs.
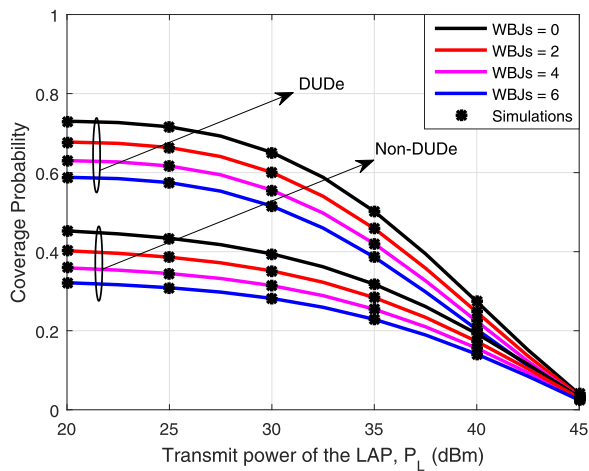

FIGURE 8. UL coverage probability against P_L, for different number of WBJs.

WBJs equal to 2, 4, and 6, respectively. Thus, the percentage decrease in the coverage probability of the decoupled access for the increase in the transmit power of WBJs from 5 dBm to 10 dBm and for the average number of WBJs equal to 2, 4, and 6, is equal to 6.25%, 11.3%, and 16.6%, respectively.

The coverage probability increases by increasing the radius of the cluster of WBJs as shown in Fig. 7. This is because of the fact that the area (for the distribution) of the WBJs within a circular disc increases by increasing the cluster radius which lowers the cumulative jamming interference at the target UE and results in the higher coverage probability in UL. For instance, the coverage probability of the decoupled access by considering the radius of the circular disc equal to 100 m and with the average number of WBJs equal to 2, 4, and 6 is equal to 0.75, 0.7, and 0.65, respectively, while, by considering the radius of the circular disc equal to 200 m, the coverage probability of the decoupled access increases up to 0.8, 0.79, and 0.78, for the average number of WBJs equal to 2, 4, and 6, respectively. Thus, for the increase in the radius of the circular disc from 100 m to 200 m and for the average number of WBJs equal to 2, 4, and 6, the percentage increase in the

coverage probability of the decoupled access is equal to 6.6%, 12.8%, and 20%, respectively.

The coverage probability decreases by increasing the transmit power of the LAP as shown in Fig. 8. This is due to the fact that by increasing the transmit power of the LAP more UEs prefer coupled association with the LAP at the cost of a decrease in the decoupled association which results in decreasing the coverage probability. Furthermore, the coverage probability of the decoupled A-HetNets decreases by increasing the average number of WBJs due to the increase in the jamming interference. For the transmit power of the LAP equal to 20 dBm, the approximate decrease in the percentage of the coverage probability of the decoupled access due to WBJ activity is equal to 6.6%, 13.3%, and 20%, for the average number of WBJs equal to 2, 4, and 6, respectively.

VI. CONCLUSION

The performance of a multi-tier A-HetNet is largely dependent on the association of the target user with the aerial platforms. This performance is further exacerbated by the jamming interference due to the presence of the WBJs. In this paper, the performance of DL and UL decoupled access along with RFA and WBJs is analyzed for the A-HetNets. The analytical expression of the coverage probability with the decoupled and the non-decoupled access is derived. The obtained results showed that the performance of the decoupled A-HetNets along with RFA is better than the non-decoupled access. However, this performance is disrupted, if WBJs are present in the vicinity. Furthermore, the performance of the decoupled access in A-HetNets improves by increasing the transmit power of the target user and the radius of the WBJ's cluster while degrades by increasing the average number of WBJs per cluster and the transmit power of the WBJs.

APPENDIX A
PROOF OF (6)

Proof: The decoupled access for the target UE located in the decoupled-enabled regions is derived as [17]

$$\mathcal{A}_D = \mathbb{P}\left\{ P_H X_H^{-\alpha_H} > P_L X_L^{-\alpha_L} \; ; \; Q_H X_H^{-\alpha_H} \le Q_L X_L^{-\alpha_L} \right\}.$$

Since $P_H > P_L$, the joint event is expressed as $\dfrac{P_L}{P_H} X_L^{-\alpha_L} < X_H^{-\alpha_H} \le \dfrac{Q_L}{Q_H} X_L^{-\alpha_L}$. Then, the association probability of the target UE is given as

$$
\mathcal{A}_D = \mathbb{P}\left\{ X_H < \left(\frac{P_H}{P_L}\right)^{\frac{1}{\alpha_H}} X_L^{\frac{\alpha_L}{\alpha_H}} \right\} \\
- \mathbb{P}\left\{ X_H < \left(\frac{Q_H}{Q_L}\right)^{\frac{1}{\alpha_H}} X_L^{\frac{\alpha_L}{\alpha_H}} \right\}
$$

$$\mathcal{H}_{v_1,w_1}^{m_1,n_1}(\gamma) \triangleq \mathcal{H}_{v_1,w_1}^{m_1,n_1}\left[\gamma \left| \begin{matrix} (a_1, A_1), \ldots, (a_{v_1}, A_{v_1}) \\ (b_1, B_1), \ldots, (b_{w_1}, B_{w_1}) \end{matrix} \right. \right] = \frac{1}{2\pi\iota} \oint_{\mathfrak{C}} \frac{\Pi_{j=1}^{m_1}\Gamma(b_j + B_j\mathfrak{s})\Pi_{j=1}^{m_1}\Gamma(1 - a_j + A_j\mathfrak{s})}{\Pi_{j=n_1+1}^{v_1}\Gamma(a_j + A_j\mathfrak{s})\Pi_{j=m_1+1}^{w_1}\Gamma(1 - b_j + B_j\mathfrak{s})} \gamma^{-\mathfrak{s}} d\gamma. \quad (22)$$

$$\overset{a}{=} \int_0^\infty \left(1 - \exp\left\{-\pi\lambda_H (P_H/P_L)^{2/\alpha_H} x^{\frac{2\alpha_L}{\alpha_H}}\right\}\right.$$

$$\left. - \left(1 - \exp\left\{-\pi\lambda_H (Q_H/Q_L)^{2/\alpha_H} x^{\frac{2\alpha_L}{\alpha_H}}\right\}\right)\right) f_{X_L}(x)dx$$

$$\overset{b}{=} 1 - 2\pi\lambda_L$$

$$\int_0^\infty \left(\frac{\alpha_H}{2\alpha_L}\mathcal{H}_{0,1}^{1,0}\left[(\sqrt{\pi\lambda_H})^{\frac{\alpha_H}{\alpha_L}}\left(\frac{P_H}{P_L}\right)^{\frac{1}{\alpha_L}} x \left| \begin{matrix} (-, -) \\ \left(0, \frac{\alpha_H}{2\alpha_L}\right) \end{matrix}\right.\right]\right.$$

$$\left. \cdot \frac{1}{2}\mathcal{H}_{0,1}^{1,0}\left[\sqrt{\pi\lambda_L}x \left| \begin{matrix} (-, -) \\ \left(0, \frac{1}{2}\right) \end{matrix}\right.\right]x\right) dx$$

$$- \left(1 - 2\pi\lambda_L \int_0^\infty \left(\frac{\alpha_H}{2\alpha_L}\mathcal{H}_{0,1}^{1,0}\right.\right.$$

$$\times \left[(\sqrt{\pi\lambda_H})^{\frac{\alpha_H}{\alpha_L}}\left(\frac{Q_H}{Q_L}\right)^{\frac{1}{\alpha_L}} x \left| \begin{matrix} (-, -) \\ \left(0, \frac{\alpha_H}{2\alpha_L}\right) \end{matrix}\right.\right]$$

$$\left.\left. \cdot \frac{1}{2}\mathcal{H}_{0,1}^{1,0}\left[\sqrt{\pi\lambda_L}x \left| \begin{matrix} (-, -) \\ \left(0, \frac{1}{2}\right) \end{matrix}\right.\right]x\right) dx\right),$$

where $\overset{a}{=}$ follows using (4), while $\overset{b}{=}$ follows by defining Fox H-function in (22), as shown at the top of the page, with values of $m_1 = 1$, $n_1 = 0$, $v_1 = 0$, and $w_1 = 1$, and using (2.9.4) of [34]. In (22), $\Gamma(t) = \int_0^\infty \mathfrak{s}^{t-1}e^{-\mathfrak{s}}d\mathfrak{s}$, γ is a complex number except zero. Furthermore, $1 \leqslant m_1 \leqslant w_1, 0 \leqslant n_1 \leqslant v_1, A_j > 0, B_j > 0$, $\mathfrak{C}$ is a complex contour, and a_j, b_j are complex numbers. Finally, (5) follows by (2.8.4) of [34]. ∎

REFERENCES

[1] *IMT Traffic Estimates for the Years 2020 to 2030*, document ITU-R M.2370-0, ITU-R Radiocommunication Sector of ITU, 2015.

[2] S. J. Nawaz, S. K. Sharma, S. Wyne, M. N. Patwary, and M. Asaduzzaman, "Quantum machine learning for 6G communication networks: State-of-the-art and vision for the future," *IEEE Access*, vol. 7, pp. 46317–46350, 2019.

[3] A. Fotouhi, H. Qiang, M. Ding, M. Hassan, L. G. Giordano, A. Garcia-Rodriguez, and J. Yuan, "Survey on UAV cellular communications: Practical aspects, standardization advancements, regulation, and security challenges," *IEEE Commun. Surveys Tuts.*, vol. 21, no. 4, pp. 3417–3442, 4th Quart., 2019.

[4] R. I. Bor-Yaliniz, A. El-Keyi, and H. Yanikomeroglu, "Efficient 3-D placement of an aerial base station in next generation cellular networks," in *Proc. IEEE Int. Conf. Commun. (ICC)*, May 2016, pp. 1–5.

[5] O. S. Oubbati, M. Atiquzzaman, P. Lorenz, M. H. Tareque, and M. S. Hossain, "Routing in flying Ad Hoc networks: Survey, constraints, and future challenge perspectives," *IEEE Access*, vol. 7, pp. 81057–81105, 2019.

[6] N. Panigrahi and S. S. Panigrahi, "Processing data acquired by a drone using a GIS: Designing a size-, weight-, and power-constrained system," *IEEE Consum. Electron. Mag.*, vol. 7, no. 2, pp. 50–54, Mar. 2018.

[7] S. Sekander, H. Tabassum, and E. Hossain, "Multi-tier drone architecture for 5G/B5G cellular networks: Challenges, trends, and prospects," *IEEE Commun. Mag.*, vol. 56, no. 3, pp. 96–103, Mar. 2018.

[8] Y. Wu, W. Fan, W. Yang, X. Sun, and X. Guan, "Robust trajectory and communication design for multi-UAV enabled wireless networks in the presence of Jammers," *IEEE Access*, vol. 8, pp. 2893–2905, 2020.

[9] B. Duan, D. Yin, Y. Cong, H. Zhou, X. Xiang, and L. Shen, "Anti-jamming path planning for unmanned aerial vehicles with imperfect jammer information," in *Proc. IEEE Int. Conf. Robot. Biomimetics (ROBIO)*, Dec. 2018, pp. 729–735.

[10] J. Miao and Z. Zheng, "Cooperative jamming for secure UAV-enabled mobile relay system," *IEEE Access*, vol. 8, pp. 48943–48957, 2020.

[11] F. Muhammad, M. S. Haroon, Z. H. Abbas, G. Abbas, and S. Kim, "Uplink interference management for HetNets stressed by clustered wide-band jammers," *IEEE Access*, vol. 7, pp. 182679–182690, 2019.

[12] M. S. Haroon, F. Muhammad, Z. H. Abbas, G. Abbas, N. Ahmed, and S. Kim, "Proactive uplink interference management for nonuniform heterogeneous cellular networks," *IEEE Access*, vol. 8, pp. 55501–55512, 2020.

[13] W. Yi, Y. Liu, A. Nallanathan, and G. K. Karagiannidis, "A unified spatial framework for clustered UAV networks based on stochastic geometry," in *Proc. IEEE Global Commun. Conf. (GLOBECOM)*, Dec. 2018, pp. 1–6.

[14] A. M. Hayajneh, S. A. R. Zaidi, D. C. McLernon, M. Di Renzo, and M. Ghogho, "Performance analysis of UAV enabled disaster recovery networks: A stochastic geometric framework based on cluster processes," *IEEE Access*, vol. 6, pp. 26215–26230, 2018.

[15] N. Cherif, M. Alzenad, H. Yanikomeroglu, and A. Yongacoglu, "Downlink coverage and rate analysis of an aerial user in integrated aerial and terrestrial networks," 2019, *arXiv:1905.11934*. [Online]. Available: http://arxiv.org/abs/1905.11934

[16] Y. Sun, T. Wang, and S. Wang, "Location optimization and user association for unmanned aerial vehicles assisted mobile networks," *IEEE Trans. Veh. Technol.*, vol. 68, no. 10, pp. 10056–10065, 2019.

[17] M. Arif, S. Wyne, K. Navaie, S. J. Nawaz, and S. H. Alvi, "Decoupled downlink and uplink access for aerial terrestrial heterogeneous cellular networks," *IEEE Access*, vol. 8, pp. 111172–111185, 2020.

[18] K. Smiljkovikj, L. Gavrilovska, and P. Popovski, "Efficiency analysis of downlink and uplink decoupling in heterogeneous networks," in *Proc. IEEE Int. Conf. Commun. Workshop (ICCW)*, Jun. 2015, pp. 125–130.

[19] L. Zhang, W. Nie, G. Feng, F.-C. Zheng, and S. Qin, "Uplink performance improvement by decoupling uplink/downlink access in HetNets," *IEEE Trans. Veh. Technol.*, vol. 66, no. 8, pp. 6862–6876, Aug. 2017.

[20] Z. Sattar, J. V. C. Evangelista, G. Kaddoum, and N. Batani, "Spectral efficiency analysis of the decoupled access for downlink and uplink in two-tier network," *IEEE Trans. Veh. Technol.*, vol. 68, no. 5, pp. 4871–4883, May 2019.

[21] K. P. Peppas, F. Lazarakis, A. Alexandridis, and K. Dangakis, "Simple, accurate formula for the average bit error probability of multiple-input multiple-output free-space optical links over negative exponential turbulence channels," *Opt. Lett.*, vol. 37, no. 15, pp. 3243–3245, 2012.

[22] A. Ijaz, S. A. Hassan, S. A. R. Zaidi, D. N. K. Jayakody, and S. M. H. Zaidi, "Coverage and rate analysis for downlink HetNets using modified reverse frequency allocation scheme," *IEEE Access*, vol. 5, pp. 2489–2502, 2017.

[23] F. Muhammad, Z. H. Abbas, G. Abbas, and L. Jiao, "Decoupled downlink-uplink coverage analysis with interference management for enriched heterogeneous cellular networks," *IEEE Access*, vol. 4, pp. 6250–6260, 2016.

[24] M. Helmy and H. Arslan, "Utilization of aerial heterogeneous cellular networks: Signal-to-interference ratio analysis," *J. Commun. Netw.*, vol. 20, no. 5, pp. 484–495, Oct. 2018.

[25] M. S. Haroon, F. Muhammad, G. Abbas, Z. H. Abbas, A. K. Hassan, M. Waqas, and S. Kim, "Interference management in ultra-dense 5G networks with excessive drone usage," *IEEE Access*, vol. 8, pp. 111172–111185, 2020.

[26] R. K. Ganti and M. Haenggi, "Interference and outage in clustered wireless ad hoc networks," *IEEE Trans. Inf. Theory*, vol. 55, no. 9, pp. 4067–4086, Sep. 2009.

[27] E. Turgut and M. C. Gursoy, "Downlink analysis in unmanned aerial vehicle (UAV) assisted cellular networks with clustered users," *IEEE Access*, vol. 6, pp. 36313–36324, 2018.

[28] S. N. Chiu, D. Stoyan, W. S. Kendall, and J. Mecke, *Stochastic Geometry and Its Applications*. Hoboken, NJ, USA: Wiley, 2013.

[29] T. D. Novlan, H. S. Dhillon, and J. G. Andrews, "Analytical modeling of uplink cellular networks," *IEEE Trans. Wireless Commun.*, vol. 12, no. 6, pp. 2669–2679, Jun. 2013.

[30] K. Smiljkovikj, H. Elshaer, P. Popovski, F. Boccardi, M. Dohler, L. Gavrilovska, and R. Irmer, "Capacity analysis of decoupled downlink and uplink access in 5G heterogeneous systems," 2014, *arXiv:1410.7270*. [Online]. Available: http://arxiv.org/abs/1410.7270

[31] J. G. Andrews, A. K. Gupta, and H. S. Dhillon, "A primer on cellular network analysis using stochastic geometry," 2016, *arXiv:1604.03183*. [Online]. Available: http://arxiv.org/abs/1604.03183

[32] L. C. Andrews and L. C. Andrews, *Special Functions of Mathematics for Engineers*. New York, NY, USA: McGraw-Hill, 1992.

[33] Y. Wang and Q. Zhu, "Modeling and analysis of small cells based on clustered stochastic geometry," *IEEE Commun. Lett.*, vol. 21, no. 3, pp. 576–579, Mar. 2017.

[34] A. A. Kilbas, *H-Transforms: Theory and Applications*. Boca Raton, FL, USA: CRC Press, 2004.

KEIVAN NAVAIE (Senior Member, IEEE) is currently with the School of Computing and Communications, Lancaster University, U.K. His research interests include provisioning dependable connectivity and positioning to intelligent cyber-physical systems. He is a Fellow of the IET, a Senior Fellow of the HEA, and a Chartered Engineer in U.K. He currently serves on the Editorial Board of the IEEE TRANSACTIONS ON WIRELESS COMMUNICATIONS, the IEEE COMMUNICATIONS LETTERS, and the IEEE COMMUNICATIONS SURVEYS AND TUTORIAL.

MOHAMMAD ARIF received the B.S. degree in electrical engineering from the University of Engineering and Technology, Peshawar, Pakistan, in 2012, and the M.S. degree in electrical engineering from COMSATS University Islamabad (CUI), Islamabad, Pakistan, in 2014, where he is currently pursuing the Ph.D. degree with the Department of Electrical and Computer Engineering.

His research interests include aerial and terrestrial heterogeneous cellular networks, dual connectivity, uplink and downlink interference management, reverse frequency allocation, indoor localization, signal processing, and channel coding.

MUHAMMAD SAJID HAROON (Graduate Student Member, IEEE) received the B.Sc. degree in electronics engineering from International Islamic University Islamabad, Pakistan, in 2007, the M.S. degree in electrical engineering from the COMSATS Institute of Information Technology, Attock, Pakistan, in 2013. He is currently pursuing the Ph.D. degree with the Ghulam Ishaq Khan Institute of Engineering Science and Technology, Swabi, Pakistan, with a focus on interference management in next-generation cellular networks using tools from stochastic geometry.

SHURJEEL WYNE (Senior Member, IEEE) received the Ph.D. degree from Lund University, Sweden, in 2009.

From 2009 to 2010, he was a Postdoctoral Research Fellow with the High-Speed Wireless Center, Lund University. Since 2010, he has been with the Department of Electrical and Computer Engineering, COMSATS University Islamabad (CUI), Islamabad, Pakistan, where he is currently an Associate Professor. His research interests include wireless channel characterization, multi-antenna systems, cooperative communications, physical layer security, and vehicular communications. He was a co-recipient of the Best Paper Award of the Antennas and Propagation Track at the IEEE VTC2013-Spring.

SADIA QURESHI received the M.S. degree in electrical engineering from the University of Engineering and Technology, Peshawar, Pakistan. She is currently pursuing the Ph.D. degree with the School of Electrical and Data Engineering, University of Technology Sydney. She is also a full-time Research Scholar with the School of Electrical and Data Engineering, University of Technology Sydney. Her research interests include heterogeneous networks, signal processing, wireless sensor networks, software-defined networking, and optical networks.

• • •